Spin-density wave in cubic γ-Fe and γ-$Fe_{100-x}Co_x$ precipitates in Cu

J. Phys.: Condens. Matter **1** (1989) 10427–10438. Printed in the UK

Spin-density wave in cubic γ-Fe and γ-$Fe_{100-x}Co_x$ precipitates in Cu

Y Tsunoda
Faculty of Science, Osaka University, Toyonaka, Osaka 560, Japan

Received 14 February 1989, in final form 30 May 1989

Abstract. An x-ray diffraction study reveals that an introduction of a small amount of Co suppresses the structural phase transition of γ-Fe precipitates in Cu and the cubic γ-FeCo alloy precipitates are available even at the lowest temperature. The magnetic structure of the cubic γ-$Fe_{100-x}Co_x$ ($x < 4$) alloy precipitates is studied by neutron diffraction, and spin-density wave (SDW) propagating along the cubic axis is found for these specimens. The Néel temperature and wavelength of the SDW decrease with increasing Co concentration. It is demonstrated that the magnetic structure of the cubic γ-Fe precipitates is also the SDW state.

1. Introduction

A quarter of a century ago, Kaufman *et al* (1963) postulated the existence of two spin states, high- and low-spin states, for FCC (γ-)Fe to explain the Invar effect of Fe–Ni alloy. Since that time, great efforts have been devoted to clarifying the magnetism of γ-Fe. Nowadays, it is recognised that the γ-Fe is located at a crossing point of ferromagnetic and antiferromagnetic states and its magnetism depends sensitively on the atomic volume. Experimentally, the high-spin γ-Fe state with large magnetic moment and large atomic volume has been studied mainly for epitaxial γ-Fe thin films grown on the Cu and Cu–Au alloy surfaces. Ferromagnetic ordering has been reported for these substances (Gradmann and Isbert 1980, Pescia *et al* 1987), but the results are still conflicting and remain unresolved (Keune *et al* 1977, Halbauer and Gonser 1983, Macedo and Keune 1988). On the other hand, the low-spin γ-Fe state has been considered to have a first-kind antiferromagnetic structure from the data of γ-Fe precipitates in Cu (Abrahams *et al* 1962) and from the extrapolation of γ-Fe alloys (Endoh and Ishikawa 1971).

Recently, the present author and colleagues found that the magnetic structure of coherent γ-Fe precipitates in Cu is more complex than that previously reported (Tsunoda *et al* 1987). This magnetic structure is stabilised by a structural phase transition occurring at a low temperature. The lattice structure in a low-temperature phase is described by the shear wave propagating along the [110] direction with the $\langle 1\bar{1}0 \rangle$ polarisation vector. Thus the local lattice structure has approximately orthorhombic symmetry. Since this structural phase transition takes place martensitically, the cubic γ-Fe precipitates with reasonable particle size are not available at low temperatures except for precipitates with sizes smaller than the critical diameter ($d_c \simeq 15$ nm). In the present paper, we report that this structural phase transition in γ-Fe precipitates in Cu is suppressed by introducing a small amount of Co which also precipitates in Cu and cubic γ-$Fe_{100-x}Co_x$ precipitates

0953-8984/89/5110427 + 12 $02.50

with a reasonable size are available. We also found that the magnetic structure of the cubic γ-**Fe**Co is a spin-density wave (SDW) state from neutron diffraction experiments. Some of the neutron diffraction data have been published previously (Tsunoda 1988). We present here experimental details of x-ray and neutron diffraction and the concentration dependence of the SDW in γ-$Fe_{100-x}Co_x$ alloys. We also demonstrate that the magnetic structure of the cubic γ-Fe precipitates is essentially the SDW state when the structural phase transition is suppressed.

2. Sample preparation and experiments

The supersaturated alloys $Cu_{97}(Fe_{100-x}Co_x)_3$ with $x = 0$–4 were melted in an induction furnace using the $Fe_{100-x}Co_x$ alloy pellets prepared in advance. Single crystals of supersaturated alloys were grown by the Bridgman method in an Ar atmosphere. After a homogenisation anneal at 1320 K for 17 h, the specimens were quenched in water. Then the precipitation anneal was performed. The aging temperature and period were fixed at 923 K for 70 h for all the specimens used to study the phase diagram. The precipitates with a spherical shape grow homogeneously in the Cu matrix. The mean diameter d of the γ-$Fe_{100-x}Co_x$ precipitates after this heat treatment is estimated to be about 50 nm using the empirical equation derived by Borrelly *et al* (1975). Although the solubility of Cu in γ-Fe has been reported to be lower than 3.5 at.% at 1123 K, it has not been accurately determined as yet (Hansen 1958). Since the aging temperature of the present specimens is rather low (923 K), the Cu content in γ-Fe is considered to be at most 1–2 at.%. The effect of Cu contamination on the magnetism of γ-Fe is not well known either but is assumed to be not serious. In this paper, we take no account of this problem when discussing the magnetism of γ-Fe and γ-$Fe_{100-x}Co_x$.

X-ray diffraction measurements were carried out using Cu $K\alpha_1$ radiation. To eliminate the Cu $K\alpha_2$ radiation and to obtain the fine experimental resolution, a Ge(111) monochromator was used. All the measurements were carried out around the 400 reciprocal lattice point.

Neutron scattering measurements were performed using the TUNS triple-axis spectrometer installed at the Japan Atomic Energy Research Institute, Tokai, Japan. The pyrolytic graphite monochromator and analyser were set to select incident and scattered neutrons of 13.7 meV. A pyrolytic graphite filter was also used to minimise $\lambda/2$ contamination. A refrigerator operated by the Solvay cycle was used for both x-ray and neutron diffraction measurements.

3. Experimental data

3.1. X-ray diffraction data

The lattice spacing of γ-$Fe_{100-x}Co_x$ precipitates is slightly smaller than that of Cu but, since the γ-$Fe_{100-x}Co_x$ particles coherently precipitate in the Cu matrix, the crystal axes of the precipitates are parallel to those of Cu. Therefore, for single-crystal specimens, the Bragg peak of the precipitates can be observed separately from that of the Cu matrix on the common axes of the scattering plane.

We studied the structural phase transition and the lattice expansion accompanied by magnetic ordering by means of the x-ray diffraction method. The temperature

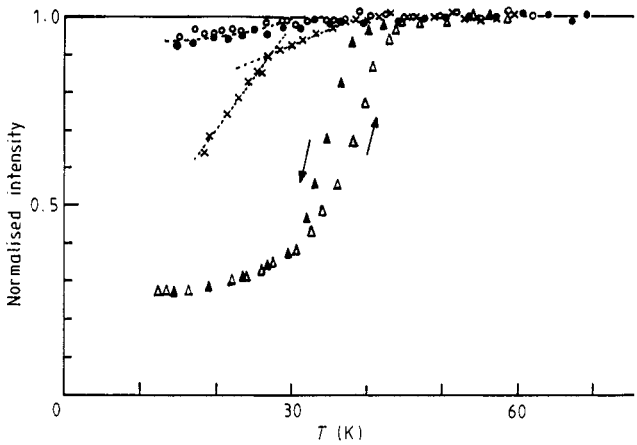

Figure 1. Temperature variations of the 400 Bragg peak intensities studied by x-ray diffraction for γ-$Fe_{99}Co_1$ (▲, △), γ-$Fe_{98.5}Co_{1.5}$ (×) and γ-$Fe_{97}Co_3$ (●, ○) precipitates in Cu.

dependence of the 400 Bragg peak intensities for γ-$Fe_{99}Co_1$, γ-$Fe_{98.5}Co_{1.5}$ and γ-$Fe_{97}Co_3$ are shown in figure 1. There are three types of temperature variation. For γ-$Fe_{99}Co_1$, the 400 Bragg peak intensity rapidly decreases with decreasing temperature, indicating that the structural phase transition to the modulated lattice structure takes place just as for pure γ-Fe precipitates (Tsunoda and Kunitomi 1988). In the second type, as observed for γ-$Fe_{98.5}Co_{1.5}$, the peak intensity varies by two steps. The first decrease in the intensity corresponds to the peak shift caused by magnetic ordering (see later discussion). The second decrease shows the start of the structural phase transition. For γ-$Fe_{97}Co_3$, only the peak shift is observed. From measurements of the full diffraction pattern of the Bragg peak, the peak shifts towards a lower scattering angle with decreasing temperature, indicating expansion of the lattice. The lattice expansion $\Delta a/a$ is roughly estimated as 4×10^{-4} for γ-$Fe_{97}Co_3$. Thus we can estimate the Néel temperature of γ-$Fe_{100-x}Co_x$ precipitates in Cu from the lattice expansion data of x-ray diffraction. The lattice spacing above the transition temperature for γ-$Fe_{100-x}Co_x$ precipitates does not depend on the Co concentration in this concentration range. The details of the structural phase transition in γ-$Fe_{100-x}Co_x$ alloy precipitates are beyond the scope of the present paper and will be published separately.

3.2. *Neutron diffraction data*

Since the experimental resolution of neutron diffraction is poorer than that of x-ray diffraction, it is impossible to separate the nuclear peaks of γ-$Fe_{100-x}Co_x$ precipitates and the Cu host. Consequently, by means of the neutron diffraction method, we studied only the magnetic structure of γ-$Fe_{100-x}Co_x$ precipitates.

The scattering intensity contour map of the 110 magnetic peak and typical diffraction pattern obtained by scanning along the [110] direction for γ-$Fe_{99.5}Co_{0.5}$ are indicated in figure 2. The 110 magnetic peak with unresolved satellite reflections on the cubic axis can be analysed in the same way as that in pure γ-Fe precipitates with a modulated lattice structure. A detailed analysis was published in the previous paper (Tsunoda *et al* 1987). We just point out here that the magnetic structure of γ-$Fe_{100-x}Co_x$ alloy precipitates

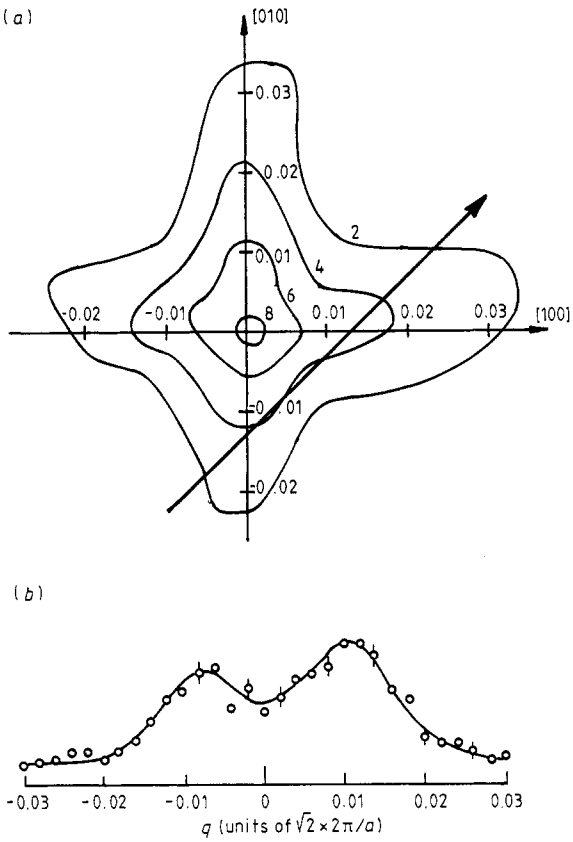

Figure 2. (*a*) Scattering intensity map of 110 magnetic peak for γ-$Fe_{99.5}Co_{0.5}$. (*b*) A typical line profile of the 110 magnetic peak obtained by scanning along the bold line indicated in the intensity map.

below the structural phase transition temperature T_m is essentially the same as that in γ-Fe precipitates with a modulated lattice structure. For the γ-$Fe_{98.5}Co_{1.5}$ specimen, both 110 and satellite peaks were observed at the lowest temperature. In figure 3, the diffraction pattern is given around the 110 reciprocal lattice point obtained by scanning along the [100] direction. Figure 4 indicates the temperature dependence of both 110 and satellite peak intensities. The satellite peaks remain up to higher temperatures. At 29 K, the 110 magnetic peak almost disappears completely, but the satellite peaks still remain. From these data, γ-$Fe_{98.5}Co_{1.5}$ precipitates in this specimen are a mixture of two phases. About half of the precipitates undergoes structural phase transition at the lowest temperature but the rest of the precipitates remain in the cubic phase. Although the mean diameter of the precipitates is about 50 nm, the particle sizes are distributed around this value. It seems that the critical diameter for the structural phase transition becomes comparable with this size at this Co concentration. Figure 5(*a*) shows a diffraction pattern for γ-$Fe_{98}Co_2$ precipitates obtained by the same scan as in figure 3. Because there is no temperature dependence of the peak intensity, the peak at 110 is ascribed to a pure $\lambda/2$ component of the Cu matrix. Careful observation shows that the central peak position deviates slightly from the exact centre of both side peaks. This is

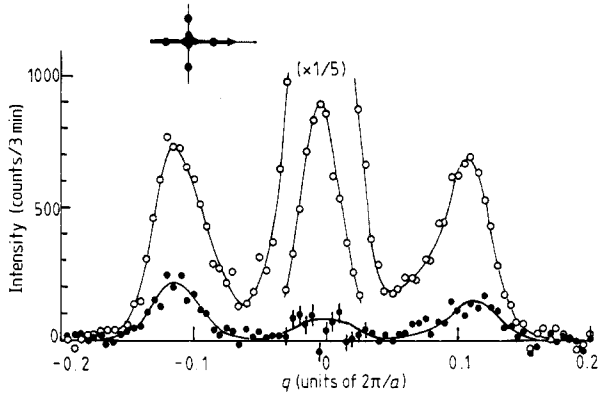

Figure 3. Diffraction pattern of the magnetic peak around the 110 reciprocal lattice point for γ-$Fe_{98.5}Co_{1.5}$. The magnetic part is determined by subtracting the data for the paramagnetic phase (○, *I* (7 K)–*I* (45 K); ●, *I* (29 K)–*I* (45 K)).

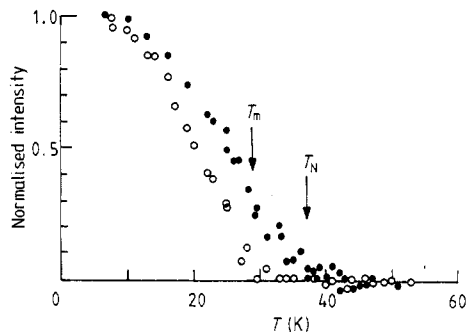

Figure 4. Temperature dependence of the 110 magnetic peak (○) and the satellite reflection (●) for γ-$Fe_{98.5}Co_{1.5}$. The 110 peak disappears at a lower temperature than the satellite peak.

due to the difference of the lattice spacings in the Cu host and γ-$Fe_{100-x}Co_x$ precipitates. The side peaks (satellite peaks) are of magnetic origin. Magnetic peaks around the 100 reciprocal lattice point were also studied. Satellite peaks were observed at $1 \pm \delta 0$ but no peaks at $1 \pm \delta 00$. All the satellite peak positions on the (001) scattering plane are depicted in figure 5(*b*). We searched for the higher harmonic components of the satellite peaks, but no peaks were observed within the experimental statistics ($I(3\boldsymbol{Q})/I(\boldsymbol{Q}) < 1.2 \times 10^{-2}$) (see figure 5(*a*)). The temperature variation of the satellite peak line profile is shown in figure 6. The shift of the satellite peak position is rather small.

The SDW wavevector is plotted as a function of Co concentration in figure 7. The wavelength of the SDW increases with decreasing Co concentration.

4. Experimental results

4.1. Magnetic phase diagram

From the x-ray and neutron diffraction data, we can determine a magnetic phase diagram of γ-$Fe_{100-x}Co_x$ precipitates in Cu for $x < 4$ as shown in figure 8. The structural phase

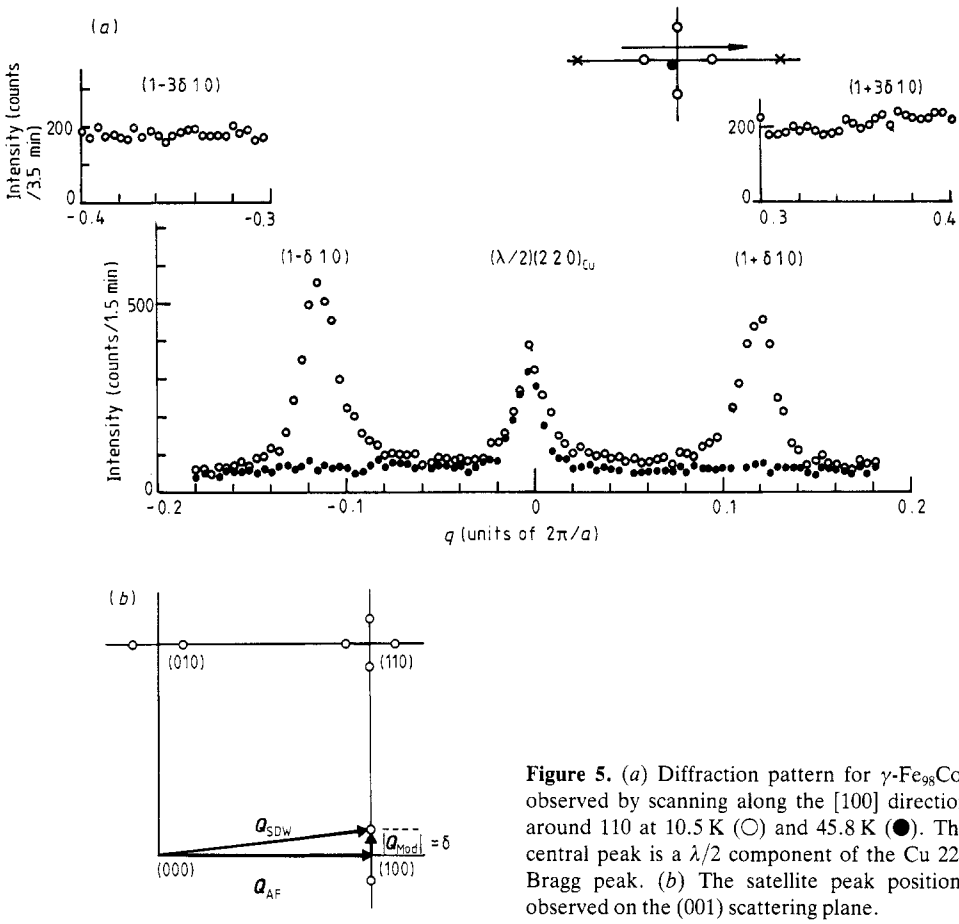

Figure 5. (*a*) Diffraction pattern for γ-$Fe_{98}Co_2$ observed by scanning along the [100] direction around 110 at 10.5 K (○) and 45.8 K (●). The central peak is a $\lambda/2$ component of the Cu 220 Bragg peak. (*b*) The satellite peak positions observed on the (001) scattering plane.

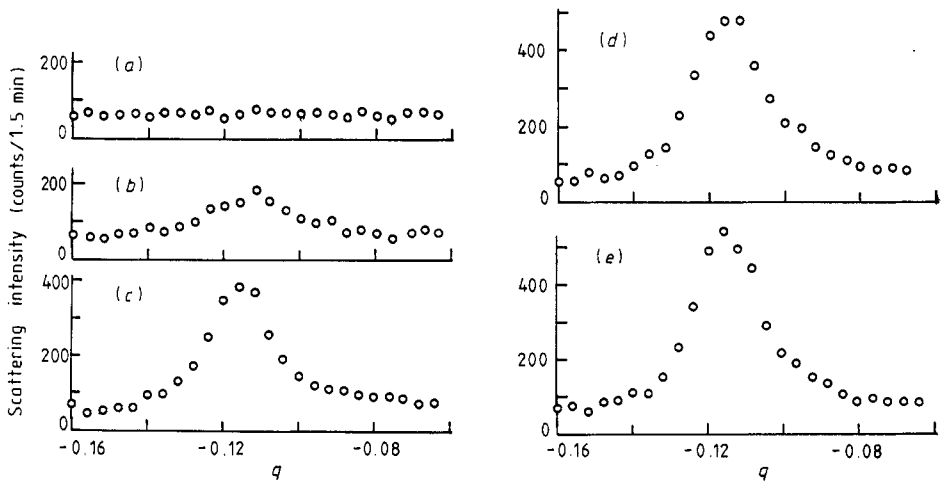

Figure 6. Temperature variation of the $(1-\delta\,1\,0)$ satellite peak diffraction pattern for γ-$Fe_{98}Co_2$ precipitates. (*a*) 48.3 K, (*b*) 30 K, (*c*) 22 K, (*d*) 16 K and (*e*) 11 K.

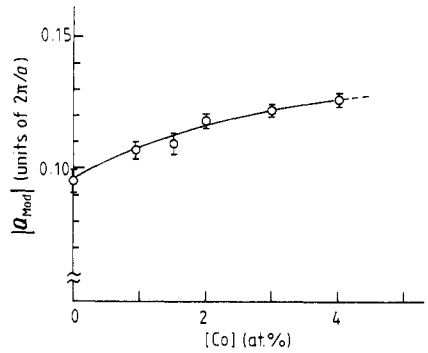

Figure 7. Concentration dependence of the SDW wavevector. The data for $x = 0$ and 1.0 are determined for the specimens with smaller-size precipitates.

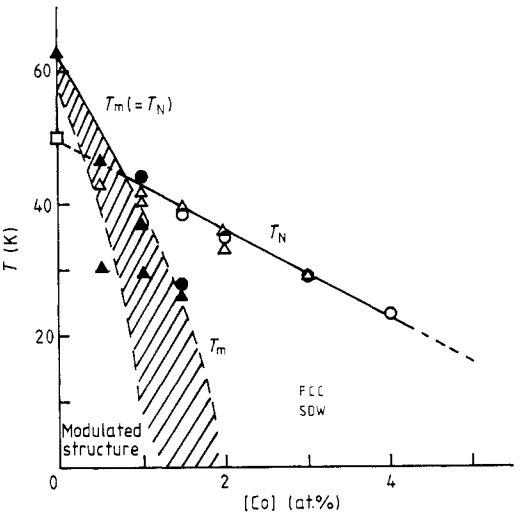

Figure 8. Phase diagram of γ-$Fe_{100-x}Co_x$ ($x < 5$) for precipitates with an average particle size of 50 nm: ▲, T_m, x-ray diffraction data; △, T_N, x-ray diffraction data; ●, T_m, neutron diffraction data; ○, T_N, neutron diffraction data; □, datum for cubic γ-Fe precipitates with a smaller size than the critical diameter; hatched region, cubic plus modulated structure.

transition temperature T_m decreases rapidly with increasing Co concentration. The T_m ($= T_N$) line splits into T_m and T_N lines at around $x \simeq 0.7$. The SDW state is stable in the cubic phase and the Néel temperature is less sensitive to the Co concentration. The data for the γ-$Fe_{99}Co_1$ specimen, which are located close to the tri-critical point, have a considerable scatter for the various specimens. Around the tri-critical point, the situation is rather complex because the structural phase transition temperature T_m in a paramagnetic phase and that in the SDW phase are different owing to the magnetoelastic coupling.

Note that this phase diagram is determined for precipitates with a mean diameter of 50 nm. As pointed out in our previous paper, T_m for pure γ-Fe precipitates depends sensitively on the precipitation particle size (Tsunoda and Kunitomi 1988). The larger the size, the higher is the transition temperature. This is valid for the γ-$Fe_{100-x}Co_x$ alloy precipitates.

4.2. *Size dependence of the SDW*

We also studied the size dependence of the Néel temperature in the SDW state. Cubic γ-$Fe_{97}Co_3$ alloy precipitates with an average diameter of 30, 50 and 80 nm were used. No

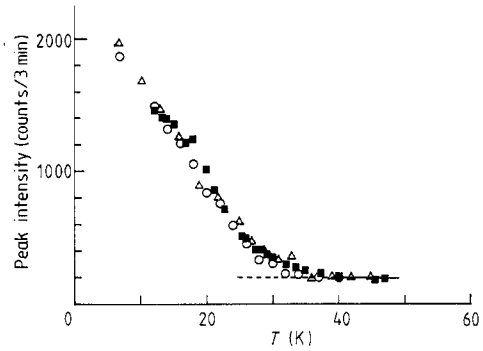

Figure 9. Comparison of the temperature dependences of the satellite peak intensities for γ-$Fe_{97}Co_3$ specimens with three different particle sizes: △, $\bar{d} = 30$ nm; ■, $\bar{d} = 50$ nm; ○, $\bar{d} = 80$ nm.

changes in the Néel temperature nor in the satellite peak position were observed. Only the linewidth for the 30 nm specimen was slightly broader than that for the other specimens. The temperature dependence of the $1 - \delta 1 0$ satellite peak intensity for these specimens is compared in figure 9 with different-size precipitates. The magnetism of the precipitates with relevant particle sizes is already free from the size effect. For the precipitates with a much smaller diameter, say $d = 5$–10 nm, the SDW formation is affected by the particle size. This problem will be published elsewhere.

4.3. Pure γ-Fe precipitates

To study the magnetic structure of pure γ-Fe precipitates in the cubic phase, the magnetic scattering of γ-Fe precipitates with a diameter smaller than the critical value ($d_c \simeq 15$ nm) were carefully measured. The magnetic part of the diffraction pattern which was obtained by subtracting the data at 65 K from those at 10 K is given in figure 10(*a*). Both diffuse satellite peaks and the 110 magnetic peak were observed. (In the previous paper (Tsunoda *et al* 1988), only the latter was reported.) These satellite peaks appeared at the same symmetry positions at those for the SDW in the γ-$Fe_{100-x}Co_x$, indicating that these satellite peaks do not come from the effect of the particle size limitation but do arise because of the SDW formation. The line broadening of satellite peaks is ascribed to the limitation of particle size. Two causes for the 110 magnetic peak are considered.

(i) The specimen contains the precipitates of both cubic and modulated lattice phases.

(ii) The lattice distortion is severe at the interface region of the precipitates and the SDW may not be stable around there.

Since no structural phase transition was observed in x-ray diffraction measurements for this specimen, the latter is more likely but, in any case, it is safe to say that the magnetic structure of cubic γ-Fe precipitates is essentially the SDW state. The temperature variation of the satellite peak intensity of γ-Fe is shown in figure 10(*b*). The open square in the phase diagram (figure 8) indicates the datum for cubic γ-Fe precipitates with a small particle size. Note that this point exists on the extrapolation of the T_N line in the cubic γ-$Fe_{100-x}Co_x$ alloys. This suggests that the magnetic properties of the precipitates with this size are almost the same as those with a diameter of 50 nm.

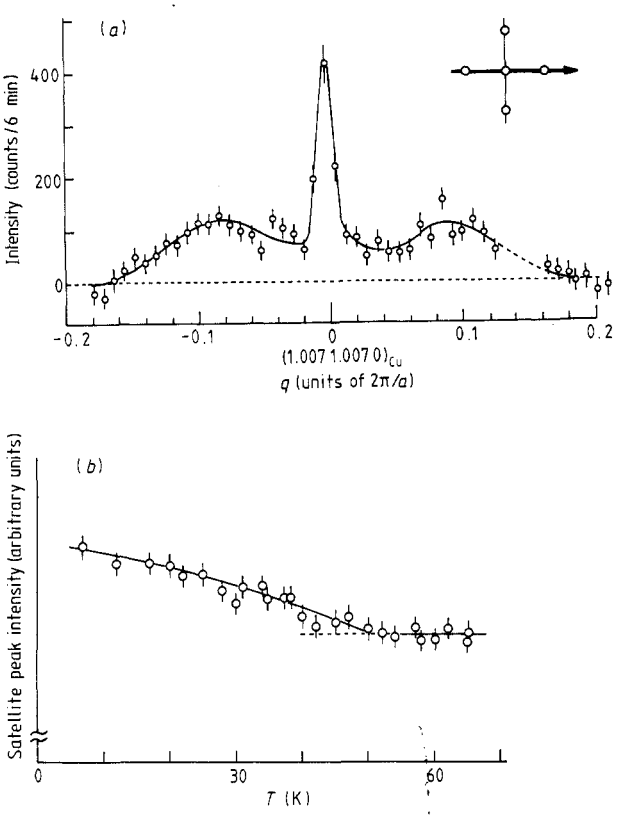

Figure 10. (*a*) Magnetic diffraction pattern (I(7 K) − I(65 K)) observed around 110 for cubic γ-Fe precipitates with a smaller size than the critical diameter. The background and λ/2 components of the 220 Bragg peak of the Cu matrix have been subtracted. (*b*) Temperature variation of the (1 − δ 1 0) satellite peak intensity for cubic γ-Fe precipitates.

4.4. *Magnetic structure of the* SDW *state*

In order to discuss the magnetic structure of the SDW state, we choose the 1δ0 satellite peak as a principal wavevector of the SDW. Then, the wavevector of the SDW $\boldsymbol{Q}_{\mathrm{SDW}}$, is written as a summation of two vectors, $\boldsymbol{Q}_{\mathrm{AF}}$ and $\boldsymbol{Q}_{\mathrm{Mod}}$, where $\boldsymbol{Q}_{\mathrm{AF}}$ is a basic antiferromagnetic wavevector $(2\pi/a\,0\,0)$ and $\boldsymbol{Q}_{\mathrm{Mod}}$ indicates a propagation vector of spin modulation with the component $(0\,\delta\,0)$ (see figure 5(*b*)). The spin structure of the SDW in γ-$Fe_{100-x}Co_x$ has to satisfy the following conditions.

(i) Spins couple antiferromagnetically in the *a*–*c* plane and have *b* and/or *c* components (no conditions for the *a* component).

(ii) Spins are modulated along the *b* axis with a period of δ.

There are still many possible magnetic structures satisfying these conditions which can be considered, including the sinusoidal spin configuration. We have searched for the satellite peaks of the strain wave (periodic lattice wave) with a wavevector of $2\boldsymbol{Q}_{\mathrm{SDW}}$ by means of the x-ray diffraction method. No appreciable peaks ($I_{\mathrm{SW}}/I_{220} < 2.3 \times 10^{-5}$) were observed at the expected positions, suggesting that the modulation of spin amplitude is very small if it even exists. If we take into consideration the fact that there is no

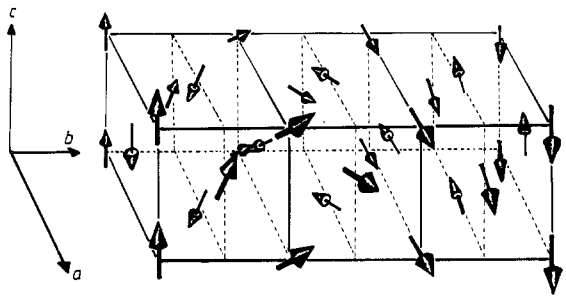

Figure 11. Helical spin structure model of the SDW in cubic γ-Fe and γ-$Fe_{100-x}Co_x$ precipitates.

third harmonic component, a helical spin configuration is a more possible structure of the SDW. One of the simplest helical structure models for the SDW in γ-$Fe_{100-x}Co_x$ is depicted in figure 11. This magnetic structure explains well the ratio of the satellite peak intensities observed around 100 and 110 if we assume an equal distribution of domains.

5. Discussion

In the epitaxial γ-Fe film grown on Cu(100), it is reported that an interface effect is limited within a few monolayers (Macedo and Keune 1988) and also the electronic structure of four-monolayer FCC Fe(100) is almost bulk like (Onellion *et al* 1986). This is consistent with the present observation for the γ-$Fe_{100-x}Co_x$ precipitates. The Néel temperature and wavevector of the SDW in cubic γ-$Fe_{100-x}Co_x$ precipitates are independent of the particle size except for extremely small particles, say $d \simeq 5$ nm. The magnetism of precipitates with a relevant size ($d \simeq 50$ nm) is free from the size effect. This is in contrast with γ-Fe precipitates for which the Néel temperature depends sensitively on the particle size (Tsunoda and Kunitomi 1988). Gonser *et al* (1963) postulated several reasons to explain the particle size dependence of the Néel temperature in γ-Fe precipitates in Cu. The problem is now solved. Although the magnetism of the precipitates is already saturated for the particles with $d \simeq 30$ nm, the structural phase transition temperature depends sensitively on the particle size, probably owing to the strain energy accumulated at the interface region. The antiferromagnetic ordering in γ-Fe precipitates is thus affected by the structural phase transition. The Néel temperature of γ-Fe precipitates at $T_N \simeq 67$ K, which has been accepted up to now, is determined by the structural phase transition via the magnetoelastic coupling. This suggests that the structural phase transition cannot have a magnetic origin. The origin of the structural phase transition will be discussed elsewhere (Tsunoda 1989). T_N for cubic γ-Fe precipitates with a small size (the γ-A state, $d < 15$ nm) lies on the T_N line extrapolated from that for cubic γ-$Fe_{100-x}Co_x$ alloys, indicating that the magnetism of the cubic γ-Fe precipitates of this size is almost like that of a bulk specimen. We can conclude that the magnetism of cubic γ-Fe precipitates is essentially the SDW state with a Néel temperature of about 50 K and a wavelength about 11 times the lattice spacing.

The spin structure given in figure 11 includes an interesting problem. As is well known, the antiferromagnetic spin configuration on the FCC lattice includes an inconsistency in itself. For instance, in the first-kind antiferromagnetic structure which has been considered to be realised in γ-Fe for a long time, eight of the nearest-neighbour spins couple in an antiparallel manner but the remaining four spins have to couple in a

parallel way. This inconsistency usually leads to lattice distortion. However, in the cubic phase, it is proposed that the triple-Q SDW state is stable (Jo and Hirai 1986). This is a non-collinear spin structure and the parallel spin component is distributed in three orthogonal directions with equal weights. In the structure given in figure 11, the basic structure is a first-kind antiferromagnetic type, but the parallel coupling on the b–c plane is partially cancelled at the cost of antiparallel coupling in another plane (the a–b plane). In total, the ferromagnetic component is cancelled by the periodic modulation. Thus the structure proposed here is regarded as another mechanism for cancelling the local inconsistency of the FCC antiferromagnet.

Theoretically, the stability of the SDW state for γ-Fe was first discussed by Hirai (1982). He derived a helical SDW ground state for γ-Fe by using a reasonable value of intra-atomic interaction. His first calculation of the susceptibility was concerned with the [100] direction. Recently, Hirai (1989) extended his work to various symmetry directions of FCC Fe. The maximum of susceptibility was obtained for the direction along [010], which is consistent with observations. However, the peak is rather broad compared with Cr, indicating that the Fermi surface nesting does not work like Cr as a mechanism of SDW stabilisation. Rather it seems to be essential that the FCC Fe is located at the crossing point of the ferromagnet and antiferromagnet in the universal magnetic phase diagram of 3D transition metals (Hirai 1982, Heine and Samson 1983).

In this connection, it should be pointed out that the satellite peak positions observed here are just the same symmetry positions as those observed in Cu–Mn spin-glass alloys (Cable *et al* 1984). In the latter, the satellite peaks never increased up to the Bragg peak owing to the disturbance due to the atomic short-range order, which favours ferromagnetic ordering. The satellite diffuse peak position, which is described as $(1\frac{1}{2} \pm \delta 0)$, shifts with Mn concentration. From the Mn concentration dependence and the similar behaviour of Ag–Mn spin-glass alloys (Ishibashi *et al* 1985), the origin of the SDW state in these spin-glass alloys is ascribed to a Fermi surface effect, such as the RKKY interaction. However, it is not clear whether an RKKY-type interaction plays an important role in the SDW state in cubic γ-Fe and γ-$Fe_{100-x}Co_x$ alloy precipitates.

The wavevector of the SDW depends on the Co concentration, although its temperature dependence is very small. Since the lattice spacings of γ-$Fe_{100-x}Co_x$ precipitates do not change appreciably in this Co concentration range, the concentration dependence in the SDW wavevector is ascribed to the band-filling effect.

Acknowledgments

The author would like to express his sincere thanks to Dr K Hirai and Dr T Jo for helpful discussions.

References

Abrahams S C, Guttman L and Kasper J S 1962 *Phys. Rev.* **127** 2052–5
Borrelly R, Pelletier J M and Pernoux E 1975 *Scr. Metall.* **9** 747–52
Cable J W, Werner S A, Felcher G P and Wakabayashi N 1984 *Phys. Rev.* B **29** 1268–78
Endoh Y and Ishikawa Y 1971 *J. Phys. Soc. Japan* **30** 1614–27
Gonser U, Meechan C J, Muir A H and Wiedersich H 1963 *J. Appl. Phys.* **34** 2373–8
Gradmann U and Isbert H O 1980 *J. Magn. Magn. Mater.* **15–8** 1109–11
Halbauer R and Gonser U 1983 *J. Magn. Magn. Mater.* **35** 55–6

Hansen M 1958 *Constitution of Binary Alloys* (New York: McGraw–Hill) p 580
Heine V and Samson J H 1983 *J. Phys. F: Met. Phys.* **13** 2155–68
Hirai K 1982 *J. Phys. Soc. Japan* **51** 1134–44
—— 1989 private communication
Ishibashi K, Tsunoda Y, Kunitomi N and Cable J W 1985 *Solid State Commun.* **56** 585–8
Jo T and Hirai K 1986 *J. Phys. Soc. Japan* **55** 2017–23
Kaufman L, Clougherty E V and Weiss R J 1963 *Acta Metall.* **11** 323–38
Keune W, Halbauer R, Gonser U, Lauer J and Williamson D L 1977 *J. Magn. Magn. Mater.* **6** 192–5
Macedo W A A and Keune W 1988 *Phys. Rev. Lett.* **61** 475–8
Onellion M F, Fu C L, Thompson M A, Erskine J L and Freeman A J 1986 *Phys. Rev.* B **33** 7322–5
Pescia D, Stampanoni M, Bona G L, Vaterlaus A, Willis R F and Weier F 1987 *Phys. Rev. Lett.* **58** 2126–9.
Tsunoda Y 1988 *J. Phys. F: Met. Phys.* **18** L251–5
—— 1989 *J. Phys. Soc. Japan* **58** 1648–54
Tsunoda Y, Imada S and Kunitomi N 1988 *J. Phys. F: Met. Phys.* **18** 1421–31
Tsunoda Y and Kunitomi N 1988 *J. Phys. F: Met. Phys.* **18** 1405–20
Tsunoda Y, Kunitomi N and Nicklow R M 1987 *J. Phys. F: Met. Phys.* **17** 2447–58